GRANULATION AND SUPERGRANULATION AS CONVECTIVE MODES IN THE SOLAR ENVELOPE

H. M. ANTIA, S. M. CHITRE, and S. K. PANDEY*
Tata Institute of Fundamental Research, Bombay 400005, India

(Received 28 April, 1980)

Abstract. The stability of linear convective modes in the solar convection zone is investigated by incorporating the mechanical and thermal effects of turbulence through the eddy transport coefficients. The inclusion of turbulent thermal conductivity and viscosity, calculated in the framework of the mixing length approximation, is demonstrated to have a profound influence on the convective growth rates. The solar envelope model of Spruit (1977) is used to show that that most rapidly growing fundamental mode and the first harmonic are in reasonable accord with the observed features of granulation and supergranulation, respectively.

1. Introduction

The velocity fields observed at the solar surface are characterized by a non-oscillatory component which is believed to be a manifestation of the convective motions in the subphotospheric layers of the Sun. The resolved motions can be ordered into three distinct classes. The granules with a characteristic cell size ~2000 km have an average life-time of the order of 8–10 min (Bahng and Schwarzschild, 1961; Namba and Diemel, 1969; Beckers and Canfield, 1976). The supergranular motions have an average diameter of ~30 000 km and life time of about 1–2 days (Simon and Leighton, 1964). Besides these two motions giant cells which are comparable in size to the total thickness of the solar convection zone have been detected (Bumba, 1970; Howard, 1971). However, the convective nature of these cells is not well established.

In an effort to understand the observed length scale and life time of granulation, Böhm (1963, 1967) calculated the growth rates of linear convective modes by perturbing the equilibrium convection zone model constructed with the mixing length formalism of Böhm–Vitense (1958). The resulting growth rates were found to increase monotonically with the decreasing length-scale well past the observed cut-off. Thus, the size distribution of cells could not be explained on the basis of Böhm's calculations. Nelson and Musman (1978) attempted to explain the absence of granules with short length-scales by invoking the damping of temperature fluctuation due to efficient horizontal radiative exchange at the surface. On the other hand, it is well known that in an optically thick medium when the radiative exchange is included, there is always a preferred length-scale for which the convective mode has a maximum growth rate (Chitre and Gokhale, 1973). Since the solar convection zone is optically thick, it is rather surprising that Böhm was not able to obtain a

* On leave of absence from Govt. Digvijai College, Rajnandgaon 491441, India.

Solar Physics **70** (1981) 67–91. 0038–0938/81/0701–0067 $06.25.

maximum growth rate and the associated preferred length-scale from his computations. We attribute this to the neglect of the turbulent conductivity in Böhm's work. In the convection zone most of the flux is carried by convective transport and the radiative conductivity is very small as compared to the turbulent heat conductivity. The turbulence is therefore expected to have a significant influence both in the way it modulates the heat flux and by the direct effect of the Reynolds stress (Spiegel, 1967). With only the radiative conductivity included in the calculation we find that the maximum growth rate ($0.012\,s^{-1}$) is attained for a length-scale of $\simeq$400 km, which is much shorter than the observed granular size.

The motivation of the present study is to extend Böhm's work by including in a crude manner the mechanical and thermal effects of turbulence in the governing hydrodynamical equations. In the absence of a satisfactory time-dependent theory of convection, we follow the prescription of Unno (1961, 1967) and parameterize the effects of turbulence through the coefficient of turbulent heat conductivity in the energy equation and through the coefficient of turbulent viscosity in the momentum equation, assuming that both are determined to a satisfactory approximation, by the mean convective velocity and the mixing length. In the solar convection zone the effect of viscosity was included by Vickers (1975) and Vandakurov (1975) while investigating the convective modes. But these model calculations were somewhat idealized and no definitive conclusions could be drawn from these studies. In his later work Böhm (1976) has attempted to incorporate the effects of turbulent heat conductivity and turbulent viscosity on convective modes in the solar convection zone. However, this study is restricted to the problem of the onset of instability. The work showed that the fundamental mode has a wavelength $\lambda \sim 1500$ km, while the wavelength corresponding to the first harmonic is around 39 000 km and these two modes were respectively identified by Böhm to represent granulation and supergranulation.

We shall attempt to account for the non-oscillatory motions observed on the solar surface in terms of the linear convective modes excited in the subsurface convection zone. Clearly, as emphasized by Simon and Weiss (1968) any satisfactory theory must explain why the distribution of cell sizes shows two distinct peaks at $\sim$2000 km and $\sim$30 000 km. The linear stability analysis should yield preferred length-scales corresponding to granulation and supergranulation, and we explore the possibility of relating these to the most unstable fundamental mode and the first harmonic.

For the present investigation we adopt for the equilibrium state the solar convection zone model of Spruit (1977) which is based on usual mixing length approximation to calculate the convective flux. It is found that the turbulent coefficients have a profound influence on the convective modes. Thus, when only the effects of turbulent heat conductivity are taken into account, the preferred length scale for the fundamental mode comes out to be $\sim$1500 km and the corresponding e-folding time of the order of 4 min. But, in addition, if the turbulent viscosity is included in the computations, depending on the choice of the turbulent Prandtl number, the

preferred sizes fall in the range 2000–3000 km with the associated e-folding time-scales varying between 5 and 10 min for the most unstable fundamental mode. Furthermore, for the same choice of parameters, the preferred diameters and the e-folding times corresponding to the first harmonic lie respectively in the range 11 000–20 000 km and 7–50 hr. It is therefore tempting to identify the fundamental mode and the first harmonic respectively with the solar granulation and supergranulation.

The plan of the paper is as follows. The mathematical formulation and the equilibrium model are set out in Section 2, and the results of the numerical computation are given in Section 3. Finally, the results are compared with the observations in Section 4.

2. Mathematical Formulation

A. BASIC EQUATIONS

We shall adopt the usual hydrodynamical equations for the conservation of mass, momentum and energy as being applicable to a viscous thermally conducting fluid. These equations in the dyadic notation take the following form:

Mass conservation:

$$\frac{\partial \rho}{\partial t} + \nabla \cdot (\rho \mathbf{v}) = 0 ;$$

momentum conservation:

$$\rho \frac{\partial \mathbf{v}}{\partial t} + \rho (\mathbf{v} \cdot \nabla)\mathbf{v} =$$

$$= \rho \mathbf{g} - \nabla P - \tfrac{2}{3}\mu \nabla (\nabla \cdot \mathbf{v}) - \tfrac{2}{3}(\nabla \cdot \mathbf{v})\nabla \mu + \nabla \cdot [\mu (\nabla \mathbf{v} + \mathbf{v}\nabla)]; \tag{1}$$

energy conservation:

$$\rho C_p \left[\frac{\partial T}{\partial t} + (\mathbf{v} \cdot \nabla) T - \nabla_{\mathrm{ad}} \frac{T}{P} \left(\frac{\partial P}{\partial t} + (\mathbf{v} \cdot \nabla) P \right) \right] = -\nabla \cdot \mathbf{F} + \Phi ,$$

where Φ is the rate of viscous dissipation,

$$\phi = \tfrac{1}{2}\mu (\nabla \mathbf{v} + \mathbf{v}\nabla) \cdot (\nabla \mathbf{v} + \mathbf{v}\nabla) - \tfrac{2}{3}\mu (\nabla \cdot \mathbf{v})^2 .$$

Here μ is the coefficient of dynamic viscosity, C_p the specific heat at constant pressure, ∇_{ad} is the logarithmic adiabatic gradient $(\partial \ln T / \partial \ln P)_{\mathrm{ad}}$, F is the total heat flux composed of the radiative flux, $\mathbf{F}^R$ and the convective flux, $\mathbf{F}^C$ and other symbols have their usual meaning. These equations must be supplemented by the equation of state. For this purpose we treat the medium as a perfect gas undergoing ionization and we also include contribution due to radiation pressure (cf. Cox and Giuli, 1968).

We have adopted the same chemical composition as used by Spruit (1977) and have included all stages of ionization for various elements by using Saha's ionization equations.

In order to compute the radiative flux we have used the Eddington approximation (cf. Ando and Osaki, 1975). It has been demonstrated by Unno and Spiegel (1966) that this approximation reduces to the exact solution of the equation of radiative transfer in the limits of large as well as small optical thickness. For the convective flux we adopt the expression given by Unno (1961) which is based on the mixing length formalism used to generate the solar equilibrium model. Thus we have

$$\mathbf{F}^R = -\frac{4}{3x\rho}\nabla J,$$

$$\mathbf{F}^C = -K_t\left(\nabla T - \nabla_{\rm ad}\frac{T}{P}\nabla P\right),$$

and so the total flux is given by

$$\mathbf{F} = -\frac{4}{3\kappa\rho}\nabla J - K_t\left(\nabla T - \nabla_{\rm ad}\frac{T}{P}\nabla P\right), \tag{2}$$

where

$$J = \sigma T^4 + \frac{C_p}{4\kappa}\left[\frac{\partial T}{\partial t} + (\mathbf{v}\cdot\nabla)T - \nabla_{\rm ad}\frac{T}{P}\left(\frac{\partial P}{\partial t} + (\mathbf{v}\cdot\nabla)P\right)\right]. \tag{3}$$

Here κ is the mean Rosseland opacity, J the intensity of radiation, K_t the coefficient of turbulent conductivity, and σ is the Stefan–Boltzmann constant. In Equation (3) if the second term on the right-hand side is neglected, the equation will reduce to an equation in the diffusion approximation, with the radiative conductivity $K_R = 16\sigma T^3/(3\kappa\rho)$. The diffusion approximation is quite good in regions well below the photosphere. However in atmospheric regions where the second term becomes comparable with the first term, the diffusion approximation is not so satisfactory.

We shall adopt the spherical geometry and as usual we assume that any physical quantity in the perturbed state can be expressed as

$$f(r, \theta, \phi, t) = f_0(r) + f_1(r) Y_l^m(\theta, \phi)\, e^{\omega t},$$

where $f_0(r)$ is the value in the unperturbed state, (r, θ, ϕ) are the spherical polar coordinates with origin at the center of the Sun, Y_l^m are the spherical harmonics, and ω the growth rate. We linearize the basic equations (1)–(3) by neglecting the higher order terms in perturbed quantities to get the following equations:

$$\tfrac{4}{3}\mu_t\frac{{\rm d}^2 v_r}{{\rm d}z^2} + \frac{{\rm d}P_1}{{\rm d}z} = \left[\frac{8\mu_t}{3r^2} + \frac{\mu_t l(l+1)}{r^2} - \frac{4}{3r}\frac{{\rm d}\mu_t}{{\rm d}z} + \rho_0\omega\right]v_r +$$

$$+\left[\frac{8\mu_t}{3r} - \frac{4}{3}\frac{{\rm d}\mu_t}{{\rm d}z}\right]\frac{{\rm d}v_r}{{\rm d}z} + \frac{l(l+1)}{r}\left[\frac{2}{3}\frac{{\rm d}\mu_t}{{\rm d}z} - \frac{7}{3r}\mu_t\right]v_h -$$

$$-\frac{l(l+1)}{3r}\mu_t\frac{\mathrm{d}v_h}{\mathrm{d}z}+g\left(\frac{\partial\rho}{\partial P}\right)_T P_1+g\left(\frac{\partial\rho}{\partial T}\right)_P T_1\,,$$

$$\mu_t\frac{\mathrm{d}^2v_h}{\mathrm{d}z^2}=\left[\frac{1}{r}\frac{\mathrm{d}\mu_t}{\mathrm{d}z}-\frac{8\mu_t}{3r^2}\right]v_r+\frac{\mu_t}{3r}\frac{\mathrm{d}v_r}{\mathrm{d}z}+$$

$$+\left[\frac{4}{3}\frac{l(l+1)}{r^2}\mu_t-\frac{1}{r}\frac{\mathrm{d}\mu_t}{\mathrm{d}z}+\omega\rho_0\right]v_h+\left[\frac{2\mu_t}{r}-\frac{\mathrm{d}\mu_t}{\mathrm{d}z}\right]\frac{\mathrm{d}v_h}{\mathrm{d}z}+\frac{1}{r}P_1\,,$$

$$-K_t\nabla_{\mathrm{ad}}\frac{T_0}{P_0}\frac{\mathrm{d}P_1}{\mathrm{d}z}+K_t\frac{\mathrm{d}T_1}{\mathrm{d}z}+\frac{4}{3\kappa_0\rho_0}\frac{\mathrm{d}J_1}{\mathrm{d}z}=$$

$$=F_r+F_0^R\left[\frac{1}{\kappa_0}\left(\frac{\partial\kappa}{\partial P}\right)_T+\frac{1}{\rho_0}\left(\frac{\partial\rho}{\partial P}\right)_T\right]P_1+F_0^R\left[\frac{1}{\kappa_0}\left(\frac{\partial\kappa}{\partial T}\right)_P+\frac{1}{\rho_0}\left(\frac{\partial\rho}{\partial T}\right)_P\right]T_1\,,$$

$$\frac{\mathrm{d}F_r}{\mathrm{d}z}=-\frac{gT_0\rho_0^2C_p}{P_0}(\nabla-\nabla_{\mathrm{ad}})v_r-\nabla_{\mathrm{ad}}\frac{T_0}{P_0}\left[\omega\rho_0C_p+\frac{l(l+1)}{r^2}K_t\right]P_1+$$

$$+\left[\omega\rho_0C_p+\frac{l(l+1)}{r^2}K_t\right]T_1+\frac{2}{r}F_r+\frac{l(l+1)}{r^2}\frac{4}{3\kappa_0\rho_0}J_1\,,$$

$$\left(\frac{1}{\rho_0}\frac{\mathrm{d}\rho_0}{\mathrm{d}z}-\frac{2}{r}\right)v_r+\frac{\mathrm{d}v_r}{\mathrm{d}z}+\frac{l(l+1)}{r}v_h-\frac{\omega}{\rho_0}\left(\frac{\partial\rho}{\partial P}\right)_T P_1-\frac{\omega}{\rho_0}\left(\frac{\partial\rho}{\partial T}\right)_P T_1=0\,,$$

$$\frac{gT_0\rho_0C_p}{4\kappa_0P_0}(\nabla-\nabla_{\mathrm{ad}})v_r+\nabla_{\mathrm{ad}}\frac{\omega T_0C_p}{4\kappa_0P_0}P_1-\left(4\sigma T_0^3+\frac{\omega C_p}{4\kappa_0}\right)T_1+J_1=0\,. \tag{4}$$

Here $F_0^R=(16\sigma T_0^3/3\kappa_0\rho_0)(\mathrm{d}T_0/\mathrm{d}z)$ is the radiative flux in the steady state, $\nabla=(\mathrm{d}\ln T/\mathrm{d}\ln P)$, and z is the depth below the level $\tau=1$. We have assumed the velocity perturbation in the form

$$\mathbf{v}(r,\theta,\phi,t)=\left(v_r(r),\, v_h(r)\frac{\partial}{\partial\theta},\, v_h(r)\frac{1}{\sin\theta}\frac{\partial}{\partial\phi}\right)Y_l^m(\theta,\phi)\,e^{\omega t} \tag{5}$$

and the perturbation $\mathbf{F}_1$ in the form

$$\mathbf{F}_1(r,\theta,\phi,t)=\left(F_r(r),\, F_h(r)\frac{\partial}{\partial\theta},\, F_h(r)\frac{1}{\sin\theta}\frac{\partial}{\partial\phi}\right)Y_l^m(\theta,\phi)\,e^{\omega t}\,. \tag{6}$$

In deriving these equations we have neglected perturbations in turbulent conductivity K_t, turbulent viscosity μ_t, and adiabatic gradient $[\nabla_{\mathrm{ad}}(T/P)]$ as well as the perturbation of the gravitation field, **g**. These assumptions are made to simplify the equations and we shall argue later that this is of no great consequence for convective growth rates. However, we have considered the perturbation in opacity due to fluctuations in the temperature and pressure in order to incorporate the effects arising from the kappa mechanism. It can be seen that the system of equations can be

written as six first order differential equations together with two auxiliary equations. The detailed derivation of these equations is given in Appendix I. For $\mu_t = 0$ and $K_t = 0$ this system of equations would be equivalent to the equations derived by Böhm (1963), provided the radiative transfer is treated in the diffusion approximation.

B. EQUILIBRIUM SOLAR MODEL

Since the convective modes are trapped in the convection zone it is sufficient to consider only the outer layers of the Sun. We have used the solar convection zone model given by Spruit (1977) which extends to approximately half the solar radius. This model is based on the usual mixing length approximation, with the mixing length $L = z + 459$ km, and the convective flux given by

$$F^C = \alpha\rho_0 C_p L W(\nabla - \nabla')\frac{T_0}{H_p}, \tag{7}$$

where the mean convective velocity W is given by

$$W = \left[\beta\frac{g}{H_p}L^2(\nabla - \nabla')\right]^{1/2}; \tag{8}$$

H_p is the pressure scale height, and ∇' refers to the logarithmic gradient (d ln T/d ln P) inside the convective element. In Spruit's model $\alpha = \frac{1}{4}$ and $\beta = \frac{1}{8}$. For the atmosphere we have used the model which is obtained by using the empirical temperature-optical depth ($T - \tau$) relation given by Vernazza *et al.* (1976). We have chosen the upper boundary a little below the temperature minimum at a level with $\tau = 7 \times 10^{-4}$ ($T \simeq 4180$ K), while the lower boundary is chosen at a depth of $\simeq 4 \times 10^5$ km ($T \simeq 4.8 \times 10^6$ K). Most of the quantities required in the equations are tabulated by Spruit. However, the partial derivatives $(\partial\rho/\partial P)_T$, $(\partial\rho/\partial T)_P$ were calculated by using the equation of state for a perfect gas undergoing ionization with the radiation pressure included (cf. Cox and Giuli, 1968). For this purpose we have used the standard chemical composition and all ionization stages of every element were included by using Saha's ionization equations. The derivatives were calculated by explicit differentiation of the equation of state. The partial derivatives of opacity $(\partial\kappa/\partial P)_T$ and $(\partial\kappa/\partial T)_P$ were calculated making use of the opacity tables of Cox and Stewart (1970), where an interpolation to Spruit's composition ($X = 0.706$, $Y = 0.280$, and $Z = 0.013$) was necessary.

Following Unno (1961) we take the turbulent heat conductivity in the form

$$K_t = \alpha\rho_0 C_p W L. \tag{9}$$

For turbulent dynamic viscosity we use the expression

$$\mu_t = P_t \alpha\rho_0 W L, \tag{10}$$

where P_t is the turbulent Prandtl number and is treated as a free parameter which should be of the order of unity. The molecular viscosity is several orders of magnitude smaller than the turbulent viscosity and hence is neglected in the problem. However, the convective velocity does not drop abruptly to zero at the boundaries of the convection zone due to penetration of convective elements into the neighbouring stable layers. In an attempt to include this effect we assume that the coefficient of turbulent dynamic viscosity μ_t drops exponentially with height in regions beyond the convection zone. The scale height for the exponential decrease in μ_t is treated as another parameter in the problem. We have taken three values of scale height 50 km, 25 km and 10 km. This applies to the region above the convection zone where penetration is appreciable. In regions below the convection zone we assume the coefficient of turbulent viscosity to have a constant value. This is good enough since the penetration of convective modes in the region below the convection zone is negligible and hence this assumption is of little consequence.

For the overlying atmospheric regions we calculated the radiative flux in the Eddington approximation, but whenever treating special cases with the diffusion approximation for these regions we have replaced the thermal conductivity K_R, by an effective value obtained by assuming the radiative flux to be constant, that is, we have taken

$$K_R = \frac{L_\odot}{\left(4\pi r^2 \frac{\mathrm{d}T_0}{\mathrm{d}z}\right)},$$

where $L_\odot$ is the total energy radiated by the Sun, which is clearly a gross underestimate. This adjustment is, however, necessary since due to a steep decrease in density and opacity in the outer regions the usual value of the radiative conductivity $K_R = 16\sigma T_0^3/3\kappa_0\rho_0$ increases steeply with height which overestimates the heat flux. Further, in these layers we have neglected the perturbation to the radiative conductivity. These modifications are of minor importance because the amplitude of convective modes is not appreciable in these layers.

C. BOUNDARY CONDITIONS

Since we have applied boundary conditions a little beyond the convection zone, the exact conditions are not very important for convective growth rates, because the amplitude of these modes falls off rapidly outside the convection zone. As will be seen from the results in the following section the boundary conditions at the lower boundary have no effect at all on the convective growth rates since the eigenfunctions decay exponentially with depth in these regions, and the existence of this boundary is not at all felt by the convective modes. However, there is a considerable penetration in the overlying region and as a result the upper boundary conditions have some effect on convective growth rates. In order to investigate the sensitivity of our results to various boundary conditions we have considered the following sets of boundary

conditions. Since the total system of equations governing the perturbations are of the sixth order we require three boundary conditions at each interface:

(I) Rigid boundaries with no momentum flux across them and maintained at constant temperature:

$$v_r = 0\,, \qquad v_h = 0\,, \quad \text{and} \quad T_1 = 0\,.$$

(II) Rigid boundaries with no momentum flux across and with the energy flux maintained constant:

$$v_r = 0, \qquad v_h = 0, \quad \text{and} \quad F_r = 0\,.$$

(III) Free boundary conditions in which the Lagrangian perturbation in pressure vanishes at the outer boundary and further the tangential components of viscous stress tensor are assumed to vanish at the boundary:

$$\omega P_1 - g\rho_0 v_r = 0\,,$$

$$v_r - r\frac{\mathrm{d}v_h}{\mathrm{d}z} - v_h = 0\,.$$

The condition on the energy flux is that its Lagrangian perturbation vanishes, i.e.,

$$\omega F_r - \frac{2F_0^R}{r} v_r = 0\,.$$

At the lower boundary the rigid conditions as in (I) are assumed.

(IV) Free boundary conditions with the thermal boundary condition demanding that the radiation does not come in from infinity. This gives

$$\frac{v_r}{\omega}\left[\frac{4}{T_0}\frac{\mathrm{d}T_0}{\mathrm{d}z} - \frac{2}{r}\right] - \frac{J_1}{\sigma T_0^4} + \frac{F_r}{F_0^R} = 0\,.$$

Other conditions are same as in (III). The conditions are the same as in (I) at the lower boundary.

D. NUMERICAL TECHNIQUE

The system of Equations (4) along with the appropriate boundary conditions defines a generalized eigenvalue problem where the eigenvalue ω is to be determined for a given value of l. For solving these equations we have used a finite difference method with explicit calculation of first order difference corrections (cf. Antia, 1979). The eigenfunctions are calculated by using an inverse iteration method. The difference correction gives an estimate of the truncation error involved in the difference approximation and was found to be very small. The convective modes have real eigenvalues and they could be easily located by looking for sign changes in the determinant of the difference equations. More accurate eigenvalues were obtained by the secant iteration method, the iteration being continued until the eigenvalue converged to 1 part in 10^5. To avoid errors due to interpolation we selected the grid

points such that we can directly use the values given in the Spruit's table. A total of 139 mesh points were used for this purpose, 92 of these mesh points were inside the convection zone while 29 points were used to cover the atmospheric region. For numerical computation we used Schwarzschild's dimensionless variables (cf. Cox and Giuli, 1968) to avoid the occurrence of very small and large numbers. The computations were carried out on DEC system 1077 employing single precision arithmetic.

3. Numerical Results

The convective modes are trapped inside the convection zone in a region with $\omega < \omega_{cr}$, where ω_{cr} is the critical growth rate (which is just the absolute value of the imaginary Brunt–Väisälä frequency) given by

$$\omega_{cr} = g\left[-\frac{T}{P}\left(\frac{\partial \rho}{\partial T}\right)_p (\nabla - \nabla_{ad})\right]^{1/2} .$$

For $\omega < \omega_{cr}$ the convective modes will have (spatially) oscillatory character, while for $\omega > \omega_{cr}$ the modes will be evanescent and the amplitude will drop exponentially with distance. Figure 1 displays ω_{cr} as a function of depth and it can be seen that ω_{cr} decays

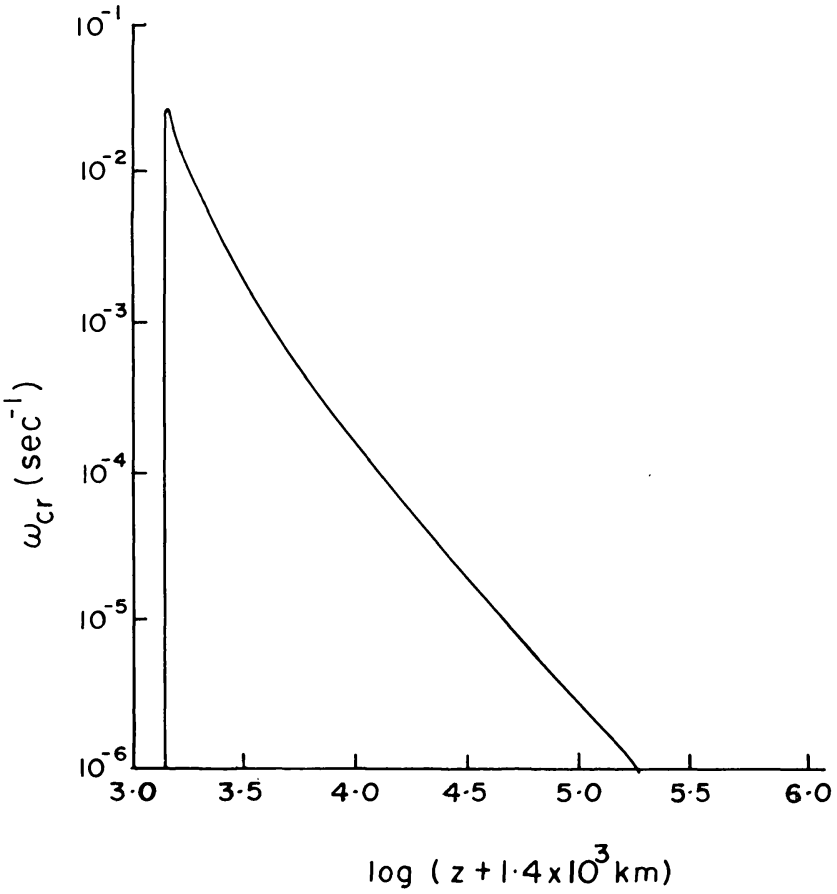

Fig. 1. The spatial variation of the critical growth rate $\omega_{cr} = g[-(T/P)(\partial\rho/\partial T)_p (\nabla - \nabla_{ad})]^{1/2}$ (s^{-1}) in the solar convection zone.

very fast with depth. Thus for any reasonable value of ω the modes will be evanescent in the lower part of the convection zone and hence their amplitude will be very small at the base of the convection zone. These modes will not penetrate appreciably beyond the convection zone. This can be verified from the behaviour of the eigenfunctions. On the other hand ω_{cr} is very large in upper regions of the convection zone and hence all modes will have propagating (oscillatory) character in the upper part of the convection zone. As a result these modes will penetrate appreciably into the overlying stable layers (where ω_{cr} is imaginary). It should be emphasised that these considerations regarding the trapping of the modes apply strictly to a situation when there is no dissipation, that is, $K_R = 0$, $K_t = 0$, and $\mu_t = 0$. For a dissipative atmosphere the condition should not be essentially different.

We have computed the growth rate ω as a function of horizontal harmonic number l. The value of l determines the horizontal wavelength of the corresponding mode,

$$\lambda = \frac{2\pi}{k_H} = \frac{2\pi R_\odot}{\sqrt{l(l+1)}},$$

where k_H is the horizontal wave number and $R_\odot$ is the solar radius. For each value of l we get a series of values of eigenvalue ω. The highest eigenvalue, the fundamental mode, is referred to as C1-mode, while the successive harmonics are referred to as C2, C3, ... For a given value of l only a finite number of modes will have positive growth rate. The negative growth rates correspond to damped modes and are of no interest to us, and we will consider only real positive eigenvalues of the system of Equations (4).

First let us consider the simplest case without any dissipative processes, that is $K_R = 0$, $K_t = 0$, and $\mu_t = 0$. Here the system of Equations (4) reduces to a second order differential equation and we require only two boundary conditions which we select to be $v_r = 0$ at both the boundaries. In this case it is found that the eigenvalues of all the harmonics increase monotonically with l as shown in Figure 2 (marked A) for the fundamental (C1) mode. Further, as l increases the eigenvalues will asymptotically reach the maximum value of ω_{cr} over the whole layer.

We shall now include only radiative conductivity K_R, but neglect the turbulent coefficients, that is set $K_t = 0$, $\mu_t = 0$ and treat the thermal dissipation in the diffusion approximation (cf. Böhm, 1963). In this case the system of Equations (4) is of the fourth order and we require two boundary conditions at each bounding surface. These we take to be

$$v_r = 0 \quad \text{and} \quad T_1 = 0$$

at both the boundaries to solve the resulting eigenvalue problem.

The results are shown by a curve marked B in Figure 2 for C1-mode. In this case the growth rate attains a maximum value of $\approx 0.012\ s^{-1}$ (e-folding time ≈ 1.4 min) for $l \approx 10\,000$ ($\lambda \approx 400$ km). This is owing to the fact that the thermal dissipation is more effective for smaller horizontal length-scales and hence the growth rate comes down at higher l. However, as noted earlier, the maximum occurs at a very small

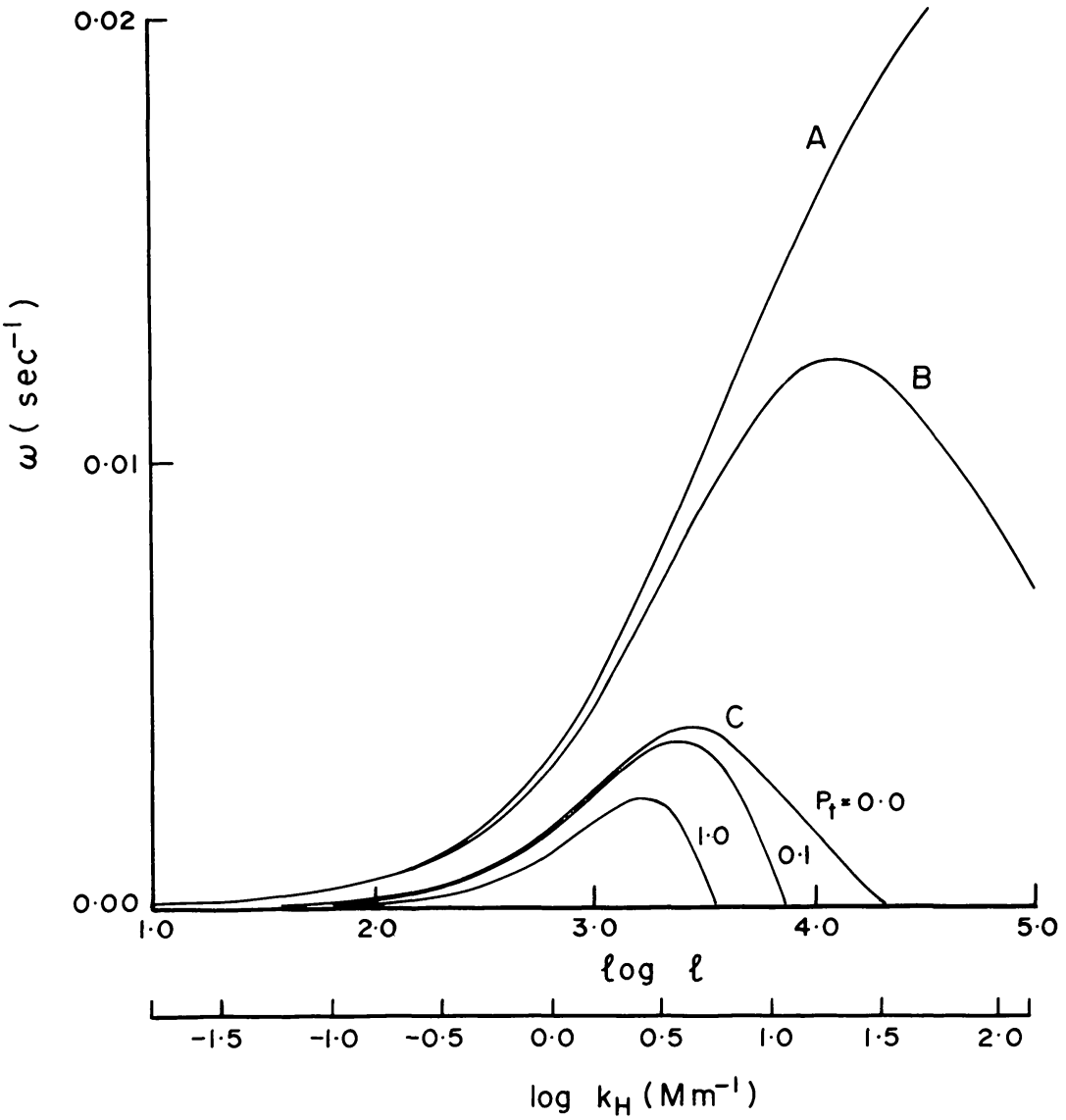

Fig. 2. The growth rate ω (s^{-1}) of the fundamental mode is shown as a function of log l for various cases: (A) Non-dissipative case with $K_R = 0$, $K_t = 0$, $\mu_t = 0$; (B) Böhm's case with $K_t = 0$, $\mu_t = 0$; and (C) with the neglect of turbulent viscosity, that is $K_t \neq 0$, $\mu_t = 0$. The other two curves refer to the fundmental mode for the turbulent Prandtl number $P_t = 0.1$ and 1.0 respectively. The horizontal wave number k_H in Mm^{-1} (logarithmic scale) is given at the bottom.

length-scale and e-folding time as compared to the observed values for solar granulation. Böhm (1963) believes that his growth rate gives a lower limit to the actual growth rate since he has overestimated the radiative dissipation in upper layers. However, we find that his growth rates yield an upper limit to the actual growth rates, since in the first place he has neglected the perturbation in convective flux which would provide an additional damping in the convection zone. Secondly, he has used the diffusion approximation which may be reasonable in the convection zone itself, but in the overlying stable layers it overestimates the thermal dissipation.

Next we include the effect of turbulent conductivity but neglect the mechanical effects due to viscosity ($\mu_t = 0$, or $P_t = 0$). In this case the governing equations are of

fourth order and we use the same set of boundary conditions, as used for the preceding case. The convective growth rate for C1-mode is shown by a curve marked C in Figure 2. In this situation we get the maximum growth rate at $l \approx 3000$ (i.e. $\lambda \approx 1500$ km, and the corresponding e-folding time is ≈ 4.2 min. This clearly demonstrates the importance of turbulent conductivity in determining the length- and time-scales of convective modes. It can be seen that for lower values the effect of K_t is not very pronounced, although, it affects the growth rates at higher values of l significantly.

We shall now consider the effect of turbulent viscosity on the convective growth rates. Figure 2 also shows the results for turbulent Prandtl number $P_t = 0.1$ and 1.0, for viscosity scale height = 10 km and with boundary conditions (I) in the Eddington

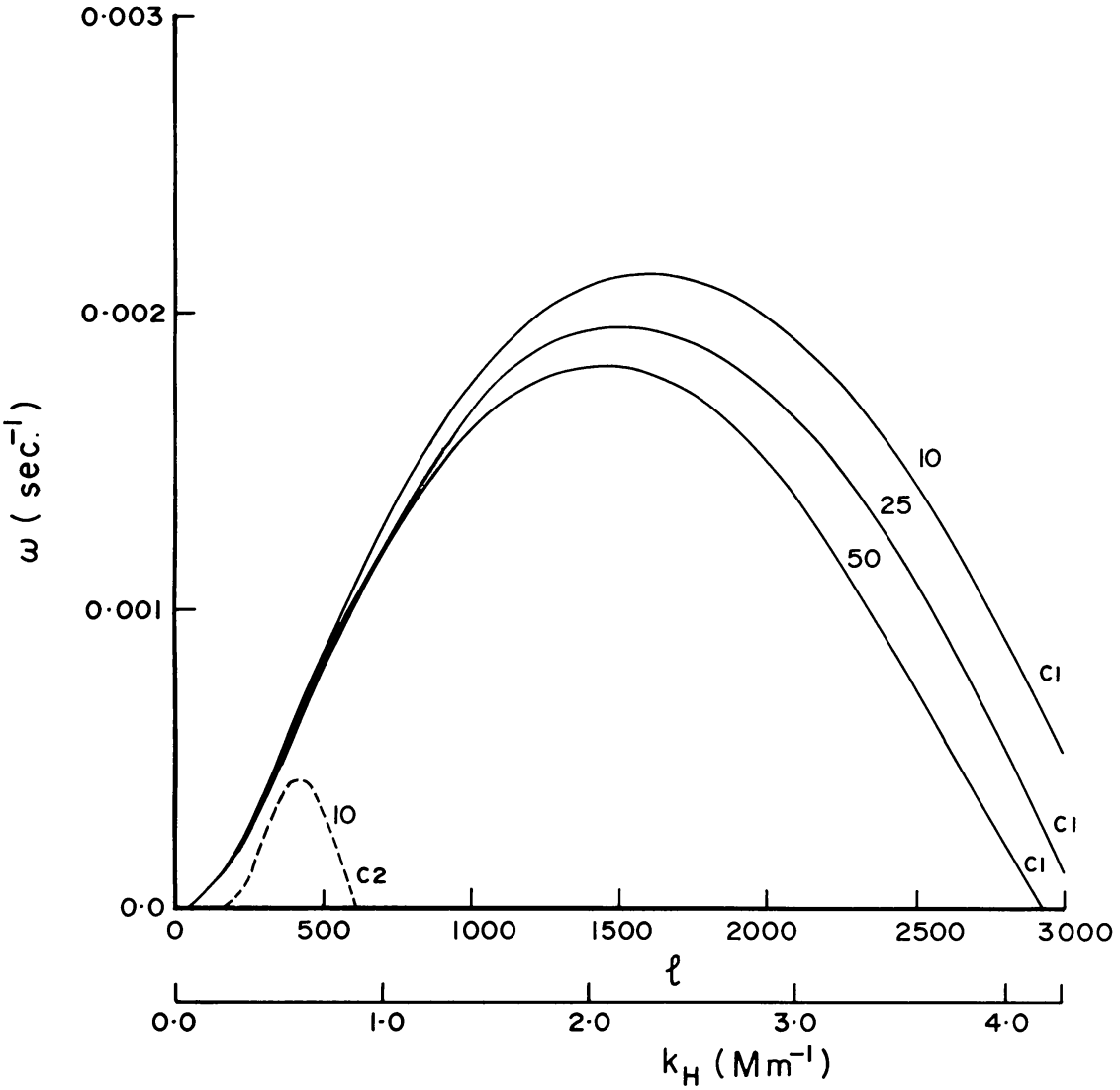

Fig. 3. The growth rate ω (s^{-1}) is shown as a function of the horizontal harmonic number l for the turbulent Prandtl number $P_t = 1.0$ for three values of viscosity scale heights in the overlying stable regions 10 km, 25 km, and 50 km. The scale at the bottom gives horizontal wave number k_H in units of Mm^{-1}. The full curves refer to the fundamental mode (C1), while the broken curve refers to the first harmonic (C2).

approximation. It can be clearly seen that the preferred wavelength as well as the corresponding e-folding time increase with the turbulent Prandtl number. An important change produced due to viscosity is that at higher values of l the growth rates become negative and hence the modes are highly damped. Further, for a given value of l, only one or two of the highest modes have positive growth rates, while the higher modes are effectively damped. Figure 3 displays convective growth rates as a function of l for $P_t = 1.0$ and three values of the viscosity scale height for the fundamental mode with the boundary conditions (I). It is clear from this figure, as we increase the viscosity scale height the viscous damping in the overlying layer will increase and hence growth rates are reduced. We also notice that the damping effect is more pronounced for larger l and higher harmonics, viz. the C2 mode is damped for viscosity scale height = 25 km and 50 km. For the rest of our numerical computation we have chosen the viscosity scale height in the overlying layers to be 10 km.

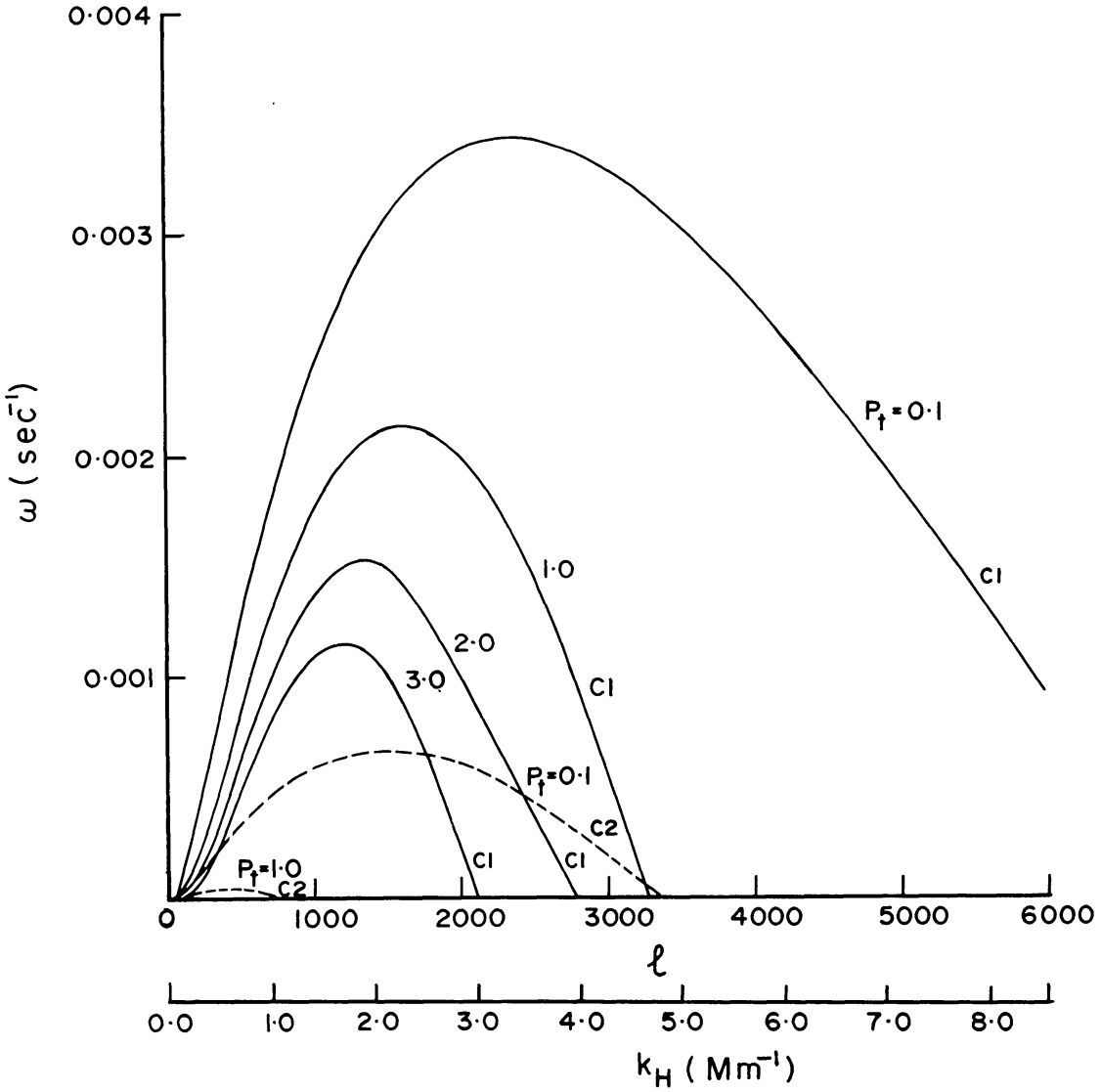

Fig. 4a. The growth rate ω (s^{-1}) of the fundamental mode (C1), shown by the full curves, and the first harmonic (C2), shown by the broken curves, is plotted against l for the turbulent Prandtl number $P_t = 0.1$, 1.0, and 2.0. The horizontal wave number k_H in units of Mm^{-1} is given at the bottom.

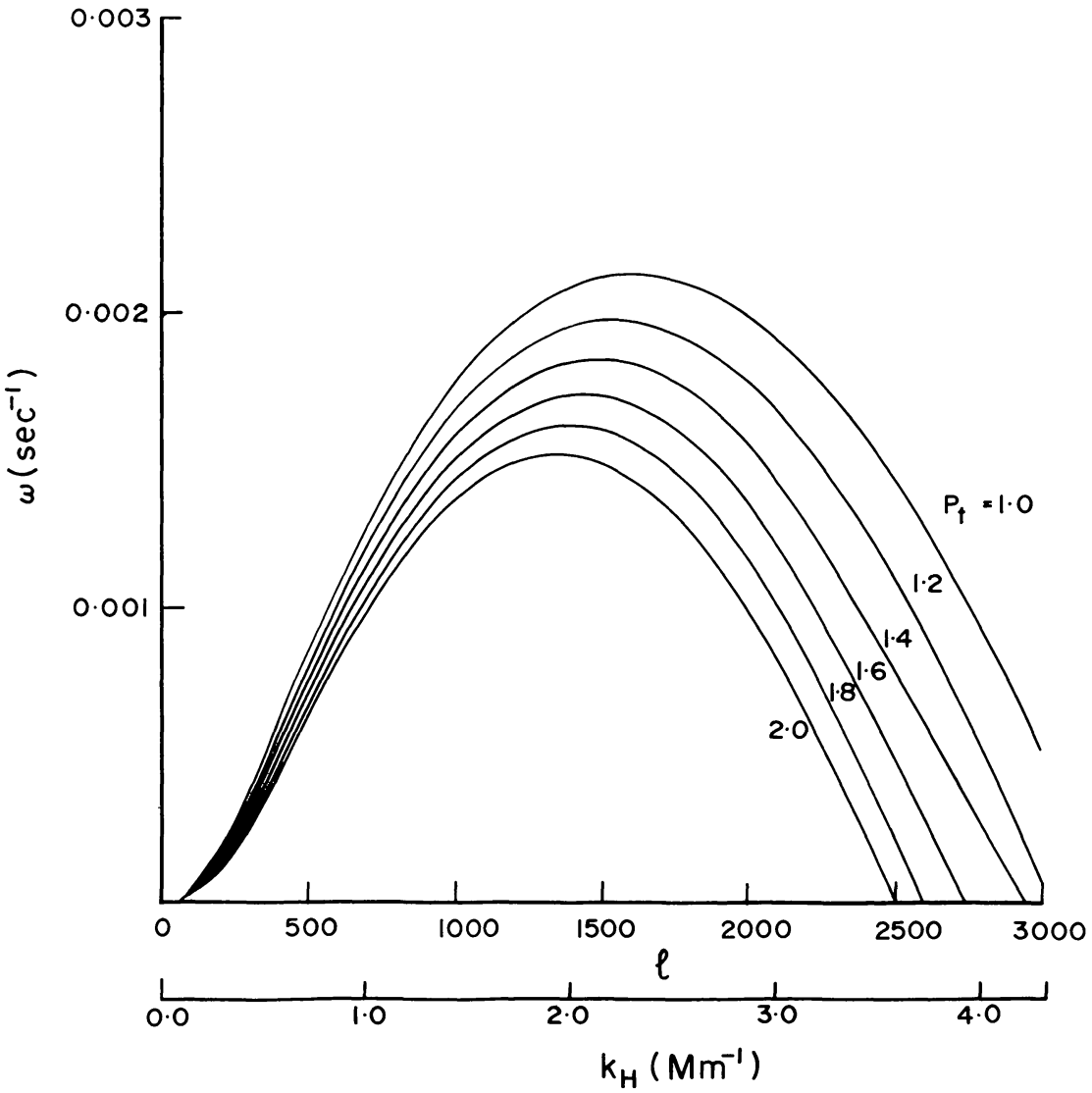

Fig. 4b. The growth rate ω (s^{-1}) of the fundamental mode is plotted as a function of l for the turbulent Prandtl number $P_t = 1.0$, 1.2, 1.4, 1.6, 1.8, and 2.0.

We have mentioned in Section 2B that the turbulent Prandtl number P_t which determines the relative importance of turbulent viscosity over the turbulent conductivity is treated as a free parameter in the present investigation. The results for a number of values of P_t for C1 and C2 modes are displayed in Figures 4 (a, b) and 5, for the first set of boundary conditions in the Eddington approximation. From these results we infer that the C2-mode has much larger horizontal wavelength and e-folding time as compared to the C1-mode. We also find the C2-mode to be far more sensitive to the turbulent Prandtl number, than the C1-mode. For example, for $P_t = 2.0$ while the C2-mode is damped, the C1-mode is still a growing mode and has a growth rate, at the maximum, somewhat smaller than it has for $P_t = 1.0$.

Let us consider the behaviour of the eigenfunctions. The eigenfunction for the C1-mode has no node in the radial velocity v_r and one node in the pressure perturbation P_1, while that for C2-mode has one node in v_r and two nodes in P_1. This

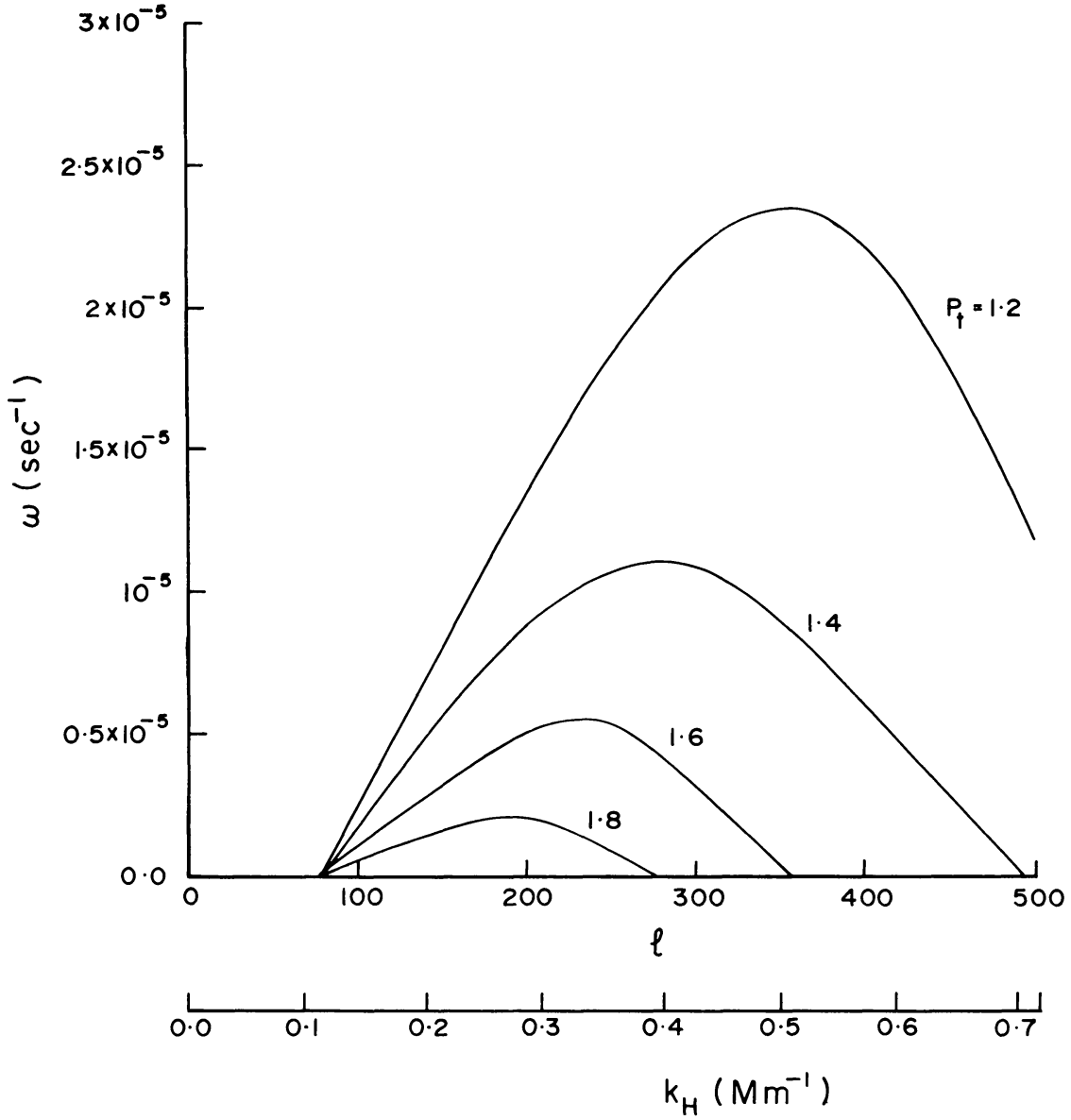

Fig. 5. The growth rate ω (s^{-1}) of the first harmonic is plotted against the horizontal harmonic number l for the turbulent Prandtl number $P_t = 1.2$, 1.4, 1.6, and 1.8. The horizontal wave number k_H in units of Mm^{-1} is given at the bottom.

behaviour is, however, not true for all the cases especially at higher l ($\gtrsim$2000). For the sake of illustration, the radial velocity eigenfunctions for few cases are shown in Figures 6 to 8. All the eigenfunctions show appreciable penetration in the stable layers above the convection zone. The eigenfunctions for C1-mode near the maximum are localized in the upper few thousand kilometers of the convection zone (see Figure 8). This is because of the rather large value of the growth rate ω for these modes, which exceeds ω_{cr} over most of the lower region of the convection zone. The eigenfunctions for C1-mode or C2-mode, for a moderate value of l ($\gtrsim$100), however, extend to a larger depth because of the smaller value of ω. The eigenfunctions for very small values of l ($\lesssim$10) extend right up to the base of the convection zone as seen from the behaviour of the eigenfunction for C1-mode

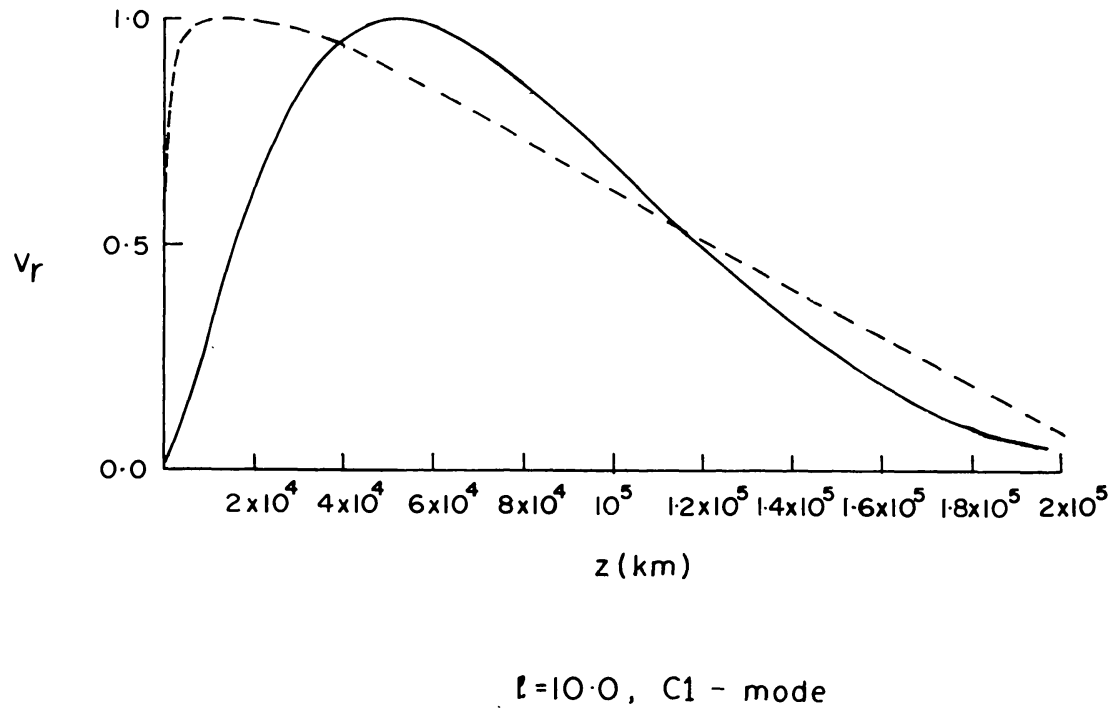

Fig. 6. The normalized radial velocity eigenfunction v_r for the fundamental mode is plotted against the geometrical depth z (km) for $l = 10$. The full curve refers to the non-adiabatic, viscous case for the turbulent Prandtl number $P_t = 1.0$, while the broken curve refers to the adiabatic, inviscid layer with $K_R = 0$, $K_t = 0$, $\mu_t = 0$.

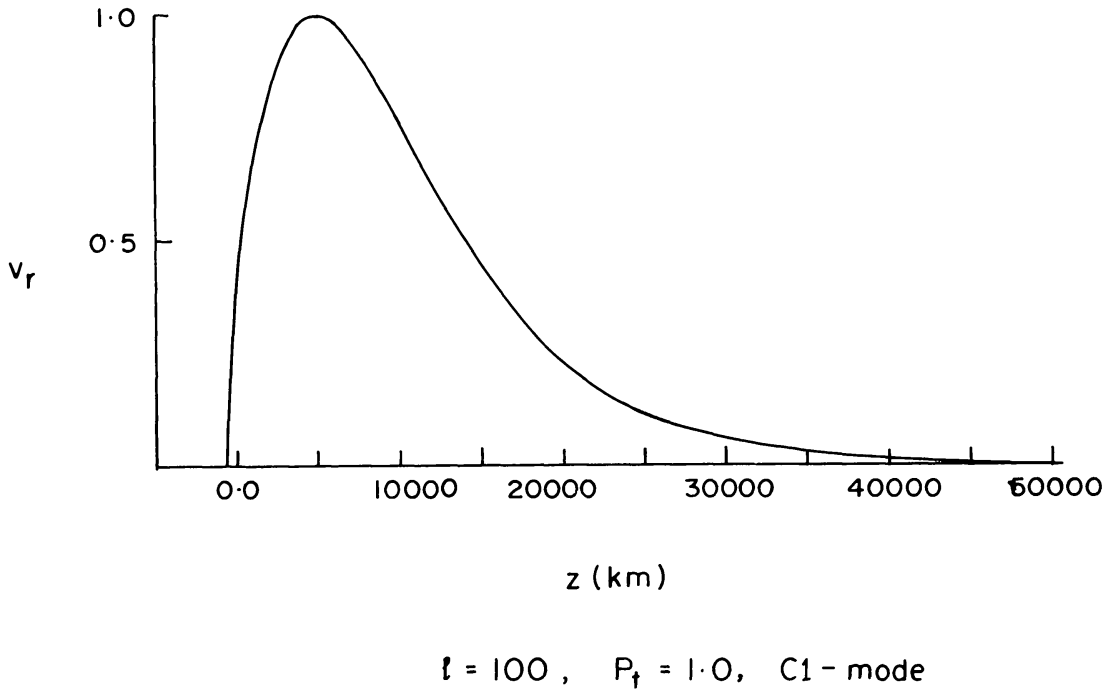

Fig. 7. The normalized radial velocity eigenfunction v_r for the fundamental mode is plotted against the geometrical depth z (km) for $l = 100$ and turbulent Prandtl number $P_t = 1.0$.

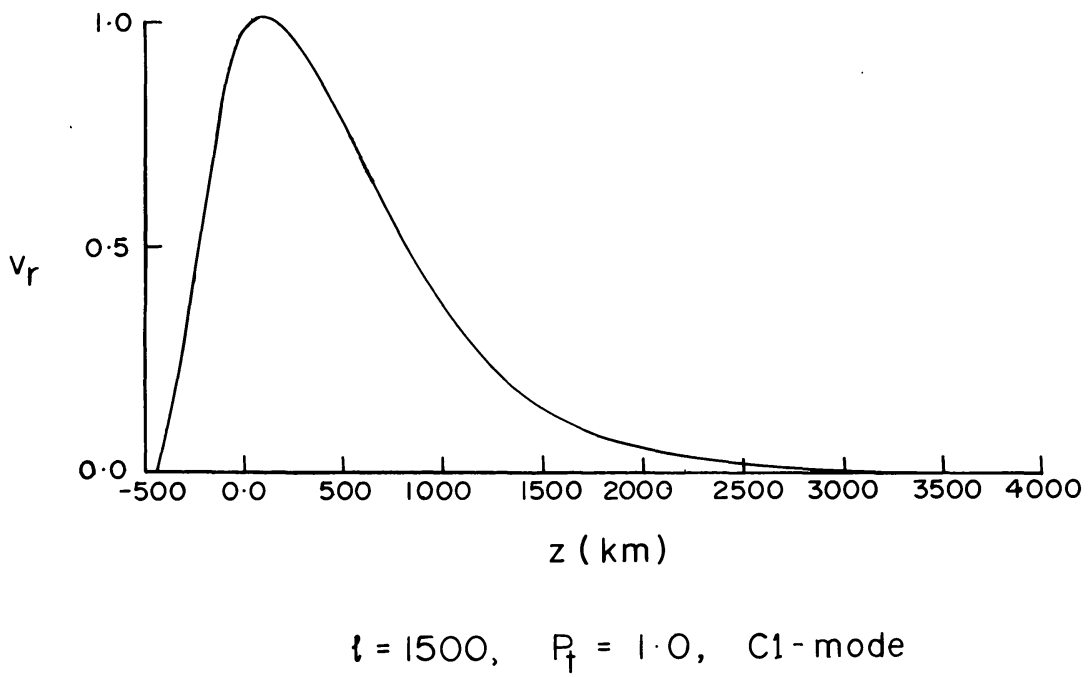

Fig. 8. The normalized radial velocity eigenfunction v_r for the fundamental mode is plotted against the geometrical depth z (km) for $l = 1500$ and the turbulent Prandtl number $P_t = 1.0$.

exhibited in Fig. 6. It may be noted that the adiabatic inviscid eigenfunction for radial velocity v_r, (shown by the broken curve in Fig. 6), peaks just below the top of the convection zone while if the dissipative processes like the turbulent heat conductivity and viscosity are included (shown by the full curve in Figure 6), the peak occurs in the deeper regions of the convective zone $z \gtrsim 50\,000$ km). Perhaps this can resolve the problem of maintaining the convective flux in the lower regions of the convection zone by a superposition of the linear modes (cf. Hart, 1973).

We shall now examine the sensitivity of our results to various approximations. Firstly, we consider the effect of neglecting perturbation in the gravitational potential $\psi(\mathbf{g}=-\nabla\psi)$. If the perturbation in ψ is included the order of governing equations increases by two and we require an additional boundary condition at each boundary which for simplicity we take to be $\psi_1 = 0$. We found that the inclusion of perturbation in ψ has hardly any influence on convective growth rates and thus the neglect of ψ_1 is justified in our computations.

Let us consider the influence of various boundary conditions on the convective growth rates. It is found that the convective growth rates are insensitive to the lower boundary conditions. As we have already seen the amplitudes of eigenfunctions become extremely small in the deeper regions and hence the growth rates show no change with respect to the boundary conditions at the lower boundary within the limits of numerical accuracy. However, the boundary conditions at the upper boundary have a small but noticeable influence on the results. Table I summarizes the results for the four sets of boundary conditions specified earlier, for $l = 100$, 1500, and 3000. It is clear that the results are not critically affected by the boundary

TABLE I

Growth rates (in s^{-1}) of the fundamental mode for various boundary conditions (I)–(IV), for $P_t = 1.0$ in the Eddington approximation

	$l = 100$	1500	3000
(I)	4.45E–5	2.12E–3	5.15E–4
(II)	4.38E–5	2.14E–3	5.17E–4
(III)	4.39E–5	2.04E–3	5.15E–4
(IV)	4.46E–5	2.14E–3	5.16E–4

conditions and therefore for the most part we have restricted the computations to the set of boundary conditions (I).

The radiative transfer of perturbations is treated using the Eddington approximation which is applicable to both the optically thick and thin disturbances. As emphasised by Unno and Spiegel (1966) the Eddington approximation is better suited to model the heat transport since in the optically thin region above the convection zone the diffusion approximation will overestimate the radiative transfer. However, since the upper layer is stable to convection this will result in an overestimate of the growth rate rather than an underestimate as one might think (cf. Pandey *et al.*, 1979). This is because of the fact that efficient thermal dissipation in the stable layer will damp out the stabilizing influence of the buoyancy forces. This can be clearly seen from Table II where we compare the results obtained with Eddington approximation with those obtained by the diffusion approximation. The diffusion approximation overestimates the growth rates although the difference in the results obtained with the two approximations is not very much except possibly at large l.

TABLE II

Growth rates (in s^{-1}) of the fundamental mode in diffusion and Eddington approximations for $P_t = 1.0$ and boundary conditions (I)

	$l = 100$	1500	3000
Diffusion approximation	4.44E–5	2.34E–3	8.33E–4
Eddigton approximation	4.45E–5	2.12E–3	5.15E–4

In these calculations we have neglected perturbations in the coefficient of dynamic viscosity μ_t, turbulent conductivity K_t, and adiabatic temperature gradient. However, we have included the perturbation in the radiative conductivity, when radiative transfer is treated in the diffusion approximation. To bring out the influence of perturbation in the radiative conductivity we neglect other dissipative processes (i.e. $K_t = 0$, $\mu_t = 0$). Table III gives convective growth rates for $l = 100$, 1000, and 10 000 for both the cases with and without the perturbation in radiative conductivity. It is clear that the convective growth rates are not critically affected by the

TABLE III

Convective growth rates (in s^{-1}) in the absence of turbulent coefficients (A) with and (B) without the perturbation of radiative conductivity in the diffusion approximation for the set of boundary conditions (I)

		$l = 100$	1000	10 000
(A)	C1	5.78E–4	4.49E–3	1.22E–2
	C2	2.66E–4	2.31E–3	8.41E–3
	C3	1.72E–4	1.55E–3	6.61E–3
	C4	9.58E–5	1.16E–3	5.48E–3
(B)	C1	4.41E–4	4.13E–3	1.16E–2
	C2	2.33E–4	2.19E–3	8.18E–3
	C3	1.59E–4	1.49E–3	6.47E–3
	C4	1.19E–4	1.12E–3	5.39E–3

perturbation in radiative conductivity. This can be understood by examining the linearized energy equation (cf. Equations (4)). It is clear that the turnover in the growth rate at high l is due to the term $[l(l+1)/r^2](4//3\kappa_0\rho_0)J_1$ (or $[l(l+1)/r^2]K_R T_1$ in the diffusion approximation). The perturbation in radiative conductivity on the other hand does not contain any l-dependent term and therefore will not contribute appreciably to l dependence of the growth rate. In the same manner perturbations in K_t, μ_t and adiabatic gradient will not contribute any l-dependent terms and hence they are unlikely to affect the convective modes significantly.

4. Conclusions

We have investigated the instability of linear convective modes for a realistic model of the solar convection zone by incorporating the mechanical and thermal effects of turbulence using the eddy transport coefficients. Admittedly, the effects of turbulence on the mean flow are taken into account very crudely by calculating in the mixing length approximation, the turbulent heat conductivity and turbulent viscosity. Nevertheless, it is hoped that such an approach would serve as a first step in our understanding of the preferred length-scales observed on the solar surface.

As a typical example we first computed the convective growth rates using the solar envelope model worked out by Spruit (1977). In Table IV we have summarized the approximate values of the most unstable convective modes for a range of turbulent Prandtl number between 0.1 and 2.0. For this choice of the parameters the e-folding times and horizontal wavelengths for the most unstable fundamental mode (C1) lie, respectively, in the range 5–11 min and 2000–3300 km. The fundamental mode does not appear to be too sensitive to the variation of the parameters, but the first harmonic (C2 mode) shows a wide variation with the e-folding times and the related wavelengths ranging between ~0.4–50 hr, and ~3000–20 000 km, respectively. Clearly the C2 mode is very sensitive to the choice of the turbulent Prandtl number. It is tempting to identify the Prandtl number P_t around 1.5 as giving the timescale and

TABLE IV

Approximate e-folding times and preferred horizontal wavelengths for the fastest growing fundamental mode (C1) and first harmonic (C2) for the set of boundary conditions (I) with Eddington approximation based on Spruit's model

	Fundamental mode (C1)		First harmonic (C2)	
P_t	e-folding time (min)	Preferred horizontal wavelength (km)	e-folding time (hr)	Preferred horizontal wavelength (km)
0.1	4.90	1900	0.43	2 900
1.0	7.84	2730	6.50	10 900
1.2	8.50	2910	11.70	12 500
1.4	9.10	3035	25.25	15 600
1.5	9.40	3060	34.70	17 500
1.6	9.63	3120	50.50	19 400
2·0	11·10	3260	–	–

the associated wavelength of the most unstable fundamental mode in reasonable agreement with the observed life-times and cell sizes of granules. For the same value of P_t, the most unstable first harmonic has e-folding time ~ 35 hr which is in accordance with the typical observed life-time for supergranules, but the related wavelength $\sim 18\,000$ km is somewhat smaller compared to the usually quoted value for the horizontal scale of $\sim 30\,000$ km for supergranulation.

With a view to test the sensitivity of the growth rates to the choice of the model for the convection zone we selected in the expression (7) for the convective flux, value of the parameter α to be equal to 1 and also the parameter β in the expression (8) for the mean convective velocity W was taken to be unity (in Spruit's model, $\alpha = \frac{1}{4}$, $\beta = \frac{1}{8}$). We have chosen the value of the mixing length L equal to the pressure scale height $H_p = (\mathrm{d}z/\mathrm{d} \ln P)$. The e-folding times and the associated horizontal wavelengths for the most rapidly growing fundamental mode and the first harmonic are set out in Table V for three sample values of the turbulent Prandtl number $P_t = 1$, 0, 1.5, and 2.0. The granular time-scale and the cell size, corresponding to $P_t \simeq 1.5$, come out to be somewhat larger for this choice of parameters compared to the corresponding values yielded by using Spruit's model, while the supergranular time scale and wavelength are found to be smaller.

It is worthwhile to point out that the linear stability analysis of the solar convection zone models adopted in this investigation neglects the contribution of the turbulent pressure. In order to examine the effect of turbulent pressure on the stability of convective modes we generated a model taking into account the contribution of isotropic turbulence to the pressure. The resulting convective growth rates for the fundmental mode and the first harmonic are slightly reduced with the inclusion of turbulent pressure which thus stabilizes the convective modes. However, the effect on the growth rates is not enough to alter the numerical results in a significant manner.

TABLE V

Approximate e-folding times and preferred horizontal wavelengths for the fastest growing fundamental model (C1) and first harmonic (C2) for the set of boundary conditions (I) with Eddington approximation based on model of the solar convection zone with $\alpha = 1$, $\beta = 1$, $L = H_p$

	Fundamental mode (C1)		First harmonic (C2)	
P_t	e-folding time (min)	Preferred horizontal wavelength (km)	e-folding time (hr)	Preferred horizontal wavelenegth (km)
1.0	11.30	3360	4.00	8 730
1.5	14.31	3640	18.80	12 540
2.0	16.70	3880	–	–

In conclusion it may be stated that for the turbulent Prandtl number of the order of unity, the e-folding time and the preferred horizontal size of the most unstable fundamental mode are in good agreement respectively with the observed life-time and length-scale of granulation. For the same value of the Prandtl number, the e-folding time and the corresponding horizontal wavelength of the preferred first harmonic are in reasonable accord with the observed life-time and scale of supergranulation. Keeping in mind the uncertainties in observations as well as in the mixing length theory our results seem to provide a natural explanation valid both for granulation and supergranulation.

Acknowledgements

It is a pleasure to acknowledge valuable conversations with Drs. E. A. Spiegel, R. Stothers and Jean-Paul Zahn. One of us (SKP) wishes to thank UGC for the award of a Teacher Fellowship and to the Director and members of Astrophysics Group of TIFR for their warm hospitality.

Appendix I

We linearize the system of Equations (1) to get the following equations governing the perturbations:

$$\omega\rho_1 + \nabla \cdot (\rho_0 \mathbf{v}) = 0\,, \tag{A1}$$

$$\omega\rho_0\mathbf{v} = \rho_1\mathbf{g} - \nabla P_1 - \tfrac{2}{3}\mu_t\nabla(\nabla\cdot\mathbf{v}) - \\ -\tfrac{2}{3}(\nabla\cdot\mathbf{v})\nabla\mu_t + \nabla\cdot[\mu_t(\nabla\mathbf{v} + \mathbf{v}\nabla)]\,, \tag{A2}$$

$$\rho_o C_p\left[\omega T_1 + (\mathbf{v}\cdot\nabla)T_0 - \nabla_{\mathrm{ad}}\frac{T_0}{P_0}(\omega P_1 + (\mathbf{v}\cdot\nabla)P_0)\right] = -\nabla\cdot\mathbf{F}_1\,, \tag{A3}$$

$$\mathbf{F}_1 = -\frac{4}{3\kappa_0\rho_0}\nabla J_1 - F_0^R\frac{\kappa_1}{\kappa_0} - F_0^R\frac{\rho_1}{\rho_0} - K_t(\nabla T_1 - \nabla_{ad}\frac{T_0}{P_0}\nabla P_1)\,, \tag{A4}$$

where

$$J_1 = 4\sigma T_0^3 T_1 + \frac{C_p}{4\kappa_0}\Big[\omega T_1 + (\mathbf{v}\cdot\nabla)T_0 - \nabla_{ad}\frac{T_0}{P_0}(\omega P_1 + (\mathbf{v}\cdot\nabla)P_0)\Big]\,,$$

$$\kappa_1 = \left(\frac{\partial\kappa}{\partial P}\right)_T P_1 + \left(\frac{\partial\kappa}{\partial T}\right)_P T_1\,, \tag{A5}$$

and

$$\rho_1 = \left(\frac{\partial\rho}{\partial P}\right)_T P_1 + \left(\frac{\partial\rho}{\partial T}\right)_P T_1\,. \tag{A6}$$

Here subscripts 0 and 1 respectively refer to the equilibrium and perturbed quantities. We choose the velocity perturbation $\mathbf{v}(r, \theta, \phi)$ and flux perturbation $\mathbf{F}_1(r, \theta, \phi)$ to be of the following form:

$$\mathbf{v}(r, \theta, \phi) = \left(v_r(r), v_h(r)\frac{\partial}{\partial\theta}, v_h(r)\frac{1}{\sin\theta}\frac{\partial}{\partial\phi}\right) Y_l^m(\theta, \phi)\,, \tag{A8}$$

$$\mathbf{F}_1(r, \theta, \phi) = \left(F_r(r), F_h(r)\frac{\partial}{\partial\theta}, F_h(r)\frac{1}{\sin\theta}\frac{\partial}{\partial\phi}\right) Y_l^m(\theta, \phi)\,. \tag{A9}$$

Further, we adopt the well-known relation for spherical harmonics, viz.

$$\left[\frac{1}{\sin\theta}\frac{\partial}{\partial\theta}\left(\sin\theta\frac{\partial}{\partial\theta}\right) + \frac{1}{\sin^2\theta}\frac{\partial^2}{\partial\phi^2}\right] Y_l^m(\theta, \phi) =$$

$$= -l(l+1)Y_l^m(\theta, \phi)\,, \tag{A10}$$

to eliminate $Y_l^m(\theta, \phi)$ from the perturbation Equations (A1–A7).

Using relations (A7), (A8), and (A10), Equation (A1) can be rewritten as

$$v_r\left[\frac{2}{r} + \frac{1}{\rho_0}\frac{\mathrm{d}\rho_0}{\mathrm{d}r}\right] + \frac{\mathrm{d}v_r}{\mathrm{d}r} + \frac{\omega}{\rho_0}\left(\frac{\partial\rho}{\partial P}\right)_T P_1 +$$

$$+\frac{\omega}{\rho_0}\left(\frac{\partial\rho}{\partial T}\right)_P T_1 - \frac{l(l+1)}{r}v_h = 0\,. \tag{A11}$$

Consider now Equation (A2) which can be written as

$$\omega\rho_0\mathbf{v} = \rho_1\mathbf{g} - \nabla P_1 + \tfrac{1}{3}\nabla(\nabla\cdot\mathbf{v}) - \tfrac{2}{3}(\nabla\cdot\mathbf{v})\nabla\mu_t +$$

$$+\mu_t\nabla^2\mathbf{v} + \nabla\mu_t\cdot(\nabla\mathbf{v} + \mathbf{v}\nabla)\,. \tag{A12}$$

Here $(\nabla\mathbf{v}+\mathbf{v}\nabla)$ is a dyadic, which in spherical polar coordinates has the following form:

$$(\nabla\mathbf{v}+\mathbf{v}\nabla)=2a_r\frac{\partial v_r}{\partial r}a_r+2a_\theta\left[\frac{1}{r}\frac{\partial v_\theta}{\partial\theta}+\frac{v_r}{r}\right]a_\theta+$$

$$+2a_\phi\left[\frac{1}{r\sin\theta}\frac{\partial v_\phi}{\partial\phi}+\frac{v_r}{r}+\frac{v_\theta}{r}\cot\theta\right]a_\phi+$$

$$+\left[\frac{1}{r}\frac{\partial v_r}{\partial\theta}+r\frac{\partial}{\partial r}\left(\frac{v_\theta}{r}\right)\right](a_ra_\theta+a_\theta a_r)+$$

$$+\left[\frac{1}{r\sin\theta}\frac{\partial v_r}{\partial\phi}+r\frac{\partial}{\partial r}\left(\frac{v_\phi}{r}\right)\right](a_ra_\phi+a_\phi a_r)+$$

$$+\left[\frac{1}{r\sin\theta}\frac{\partial v_\theta}{\partial\phi}+\frac{\sin\theta}{r}\frac{\partial}{\partial\theta}\left(\frac{v_\phi}{\sin\theta}\right)\right](a_\theta a_\phi+a_\phi a_\theta)\,, \tag{A13}$$

where (v_r, v_θ, v_ϕ) are the components of $\mathbf{v}$ and (a_r, a_θ, a_ϕ) those of a unit vector $\mathbf{a}$ in spherical geometry.

The product $\nabla\mu_t\cdot(\nabla\mathbf{v}+\mathbf{v}\nabla)$, using (A13) and remembering that the dynamic viscosity μ_t is a function of r only, can be written as

$$\nabla\mu_t\cdot(\nabla\mathbf{v}+\mathbf{v}\nabla)=2\frac{\mathrm{d}\mu_t}{\mathrm{d}r}\frac{\partial v_r}{\partial r}a_r+$$

$$+\frac{\mathrm{d}\mu_t}{\mathrm{d}r}\left[\frac{1}{r}\frac{\partial v_r}{\partial\theta}+r\frac{\partial}{\partial r}\left(\frac{v_\theta}{r}\right)\right]a_\theta+$$

$$+\frac{\mathrm{d}\mu_t}{\mathrm{d}r}\left[\frac{1}{r\sin\theta}\frac{\partial v_r}{\partial\phi}+r\frac{\partial}{\partial r}\left(\frac{v_\phi}{r}\right)\right]a_\phi\,. \tag{A14}$$

Using (A7), (A8), (A10), and (A14), Equation (A12) can be separated into its radial and horizontal components, which after simplification, can be cast as follows:

(i) The radial component:

$$\frac{4}{3}\mu_t\frac{\mathrm{d}^2v_r}{\mathrm{d}r^2}-\frac{dP_1}{\mathrm{d}r}=\left[\frac{8}{3r^2}\mu_t+\frac{4}{3r}\frac{\mathrm{d}\mu_t}{\mathrm{d}r}+\mu_t\frac{l(l+1)}{r^2}+\rho_0\omega\right]v_r-$$

$$-\left[\frac{8}{3r}\mu_t+\frac{4}{3}\frac{\mathrm{d}\mu_t}{\mathrm{d}r}\right]\frac{\mathrm{d}v_r}{\mathrm{d}r}-$$

$$-\left[\frac{7}{3}\mu_t\frac{l(l+1)}{r^2}+\frac{2}{3}\frac{\mathrm{d}\mu_t}{\mathrm{d}r}\frac{l(l+1)}{r}\right]v_h+$$

$$+\frac{1}{3}\mu_t\frac{l(l+1)}{r}\frac{\mathrm{d}v_h}{\mathrm{d}r}+g\left(\frac{\partial\rho}{\partial P}\right)_T P_1+g\left(\frac{\partial\rho}{\partial T}\right)_P T_1\,, \tag{A15}$$

and (ii) the horizontal component:

$$\mu_t \frac{d^2 v_h}{dr^2} = -\left[\frac{8}{3}\frac{\mu_t}{r^2} + \frac{1}{r}\frac{d\mu_t}{dr}\right] v_r - \frac{1}{3r}\mu_t \frac{dv_r}{dr} +$$
$$+\left[\frac{4}{3}\mu_t \frac{l(l+1)}{r^2} + \frac{1}{r}\frac{d\mu_t}{dr} + \rho_0 \omega\right] v_h -$$
$$-\left[\frac{2}{r}\mu_t + \frac{d\mu_t}{dr}\right]\frac{dv_h}{dr} + \frac{1}{r} P_1 . \tag{A16}$$

We now consider the energy flux Equations (A3–A5). Using the expression (A9) for $\mathbf{F}_1$ we can write

$$-\nabla \cdot \mathbf{F}_1 = -\frac{1}{r^2}\frac{d}{dr}(r^2 F_r) + \frac{l(l+1)}{r} F_h . \tag{A17}$$

Further, Equation (A4) can be separated into its radial and horizontal components to get

$$F_r = -\frac{4}{3\kappa_0 \rho_0}\frac{dJ_1}{dr} - F_0^R \frac{\kappa_1}{\kappa_0} - F_0^R \frac{\rho_1}{\rho_0} - K_t\left(\frac{dT_1}{dr} - \nabla_{ad}\frac{T_0}{P_0}\frac{dP_1}{d\gamma}\right), \tag{A18}$$

and

$$F_h = -\frac{4}{3\kappa_0 \rho_0}\frac{J_1}{r} - K_t\left(\frac{T_1}{r} - \nabla_{ad}\frac{T_0}{\rho_0}\frac{P_1}{r}\right), \tag{A19}$$

neglecting the perturbation in the turbulent conductivity K_t and the adiabatic gradient $\nabla_{ad}(T/P)$. Using (A17) and (A19) and Equation (A3), we obtain the following equation:

$$\frac{dF_r}{dr} = \rho_0^2 C_p g \frac{T_0}{P_0}(\nabla - \nabla_{ad}) v_r - \left[\frac{l(l+1)}{r^2} K_t + \rho_0 C_p \omega\right] T_1 +$$
$$+\nabla_{ad}\frac{T_0}{P_0}\left[\frac{l(l+1)}{r^2} K_t + \rho_0 C_p \omega\right] P_1 - \frac{2}{r} F_r - \frac{4}{3\kappa_0 \rho_0}\frac{l(l+1)}{r^2} J_1 . \tag{A20}$$

Equation (A18) can be further simplified by using the expressions for κ_1 (using (A6)) and ρ_1 (using (A7)) and can be expressed as

$$K_t \frac{dT_1}{dr} - K_t \nabla_{ad}\frac{T_0}{P_0}\frac{dP_1}{dr} + \frac{4}{3\kappa_0 \rho_0}\frac{dJ_1}{dr} =$$
$$= -F_0^R\left[\frac{1}{\kappa_0}\left(\frac{\partial \kappa}{\partial P}\right)_T + \frac{1}{\rho_0}\left(\frac{\partial \rho}{\partial P}\right)_T\right] P_1 -$$
$$-F_0^R\left[\frac{1}{\kappa_0}\left(\frac{\partial \kappa}{\partial T}\right)_P + \frac{1}{\rho_0}\left(\frac{\partial \rho}{\partial t}\right)_P\right] T_1 - F_r . \tag{A21}$$

The relation connecting J_1 and T_1 is provided by Equation (A5), which on simplification reduces to

$$J_1 - \left[4\sigma T_0^3 + \frac{C_p\omega}{4\kappa_0}\right] T_1 + \frac{C_p\omega}{4\kappa_0}\nabla_{ad}\frac{T_0}{P_0}P_1 +$$

$$+ \frac{C_p\rho_0 g T_0}{4\kappa_0 P_0}(\nabla - \nabla_{ad})v_r = 0 . \qquad \text{(A22)}$$

Thus, finally equations governing the perturbations are (A11), (A15), (A16), (A20), (A21), and (A22), with r as the independent variable. On employing the transformation $r = (R_\odot - z)$ we recover the system of Equations (4) given in Section 2 with z as the independent variable.

References

Ando, H. and Osaki, Y.: 1975, *Publ. Astron. Soc. Japan* **27**, 581.

Antia, H. M.: 1979, *J. Computational Phys.* **30**, 283.

Bahng, J. D. and Schwarzschild, M.: 1961, *Astrophys. J.* **134**, 312.

Beckers, J. M. and Canfield, R. C.: in R. Cayrel and M. Steinberg (eds.), *Physique des Mouvements dans les Atmospheres Stellaires*, Colloques Internationaux du C.N.R.S. No. 250.

Böhm, K. H.: 1963, *Astrophys. J.* **137**, 881.

Böhm, K. H.: 1967, in R. N. Thomas (ed.), 'Aerodynamic Phenomena in Stellar Atmospheres', *IAU Symp.* **28**, 366.

Böhm, K. H.: 1976, in R. Cayrel and M. Steinberg (eds.), *Physique des Mouvements dans les Atmospheres Stellaires*, Colloques Internationaux du C.N.R.S. No. 250.

Böhm-Vitense, K. E.: 1958, *Z. Astrophys.* **46**, 108.

Bumba, V.: 1970, *Solar Phys.* **14**, 80.

Chitre, S. M. and Gokhale, M. H.: 1973, *Solar Phys.* **30**, 319.

Cox, J. P. and Guili, R. T.: 1968, *Principles of Stellar Structure*, Gordon and Breach, Science Publishers.

Cox, J. P. and Stewart, J. H.: 1970, *Astrophys. J. Suppl.* **19**, 243.

Hart, M. H.: 1973, *Astrophys. J.* **184**, 587.

Howard, R.: 1971, *Solar Phys.* **16**, 21.

Namba, O. and Diemel, W. E.: 1969, *Solar Phys.* **7**, 167.

Nelson, G. D. and Musman, S.: 1978, *Astrophys. J.* **D22**, L69.

Pandey, S. K., Antia, H. M., and Chitre, S. M.: 1979, *Astrophys. Space Sci.* **63**, 103.

Simon, G. W. and Leighton, R. B.: 1964, *Astrophys. J.* **40**, 1120.

Simon, G. W. and Weiss, N. O.: 1968, *Z. Astrophys.* **69**, 435.

Spiegel, E. A.: 1967, in R. N. Thomas (ed.), 'Aerodynamic Phenomena in Stellar Atmospheres', *IAU Symp.* **28**, 348.

Spruit, H. C.: 1977, Ph.D. Thesis, Utrecht.

Unno, W.: 1961, *Publ. Astron. Soc. Japan* **13**, 276.

Unno, W.: 1967, *Publ. Astron. Soc. Japan* **19**, 140.

Unno, W. and Spiegel, E. A.: 1966, *Publ. Astron. Soc. Japan* **18**, 285.

Vandakurov, Yu. V.: 1975, *Solar Phys.* **40**, 3.

Vernazza, J. E., Avrett, E. H., and Loeser, R.: 1976, *Astrophys. J. Suppl.* **30**, 1.

Vickers, G. T.: 1971, *Astrophys. J.* **163**, 363.